Enhancing Tool Life in High-Speed Machining of Compacted Graphite Iron (CGI) Using Controlled Modulation

Y. Guo, J. B. Mann, H. Yeung & S. Chandrasekar

Tribology Letters

ISSN 1023-8883
Volume 47
Number 1

Tribol Lett (2012) 47:103-111
DOI 10.1007/s11249-012-9966-z

Springer

Tribol Lett (2012) 47:103–111
DOI 10.1007/s11249-012-9966-z

ORIGINAL PAPER

Enhancing Tool Life in High-Speed Machining of Compacted Graphite Iron (CGI) Using Controlled Modulation

Y. Guo · J. B. Mann · H. Yeung · S. Chandrasekar

Received: 5 January 2012 / Accepted: 16 April 2012 / Published online: 29 April 2012

Abstract The application of controlled, low-frequency modulation superimposed onto the cutting process—modulation-assisted machining (MAM)—is shown to be quite effective in reducing the wear of cubic boron nitride (CBN) tools when machining compacted graphite iron (CGI) at high machining speeds (>500 m/min). The tool life is at least one order of magnitude greater than that in conventional machining. The improvement in wear performance is a consequence of a reduction in the severity of the tool–work contact conditions in MAM: reduction in intimacy of the contact, formation of discrete chips, enhanced fluid action, and lower cutting temperatures. The propensity for thermochemical wear of CBN, the principal wear mode at high speeds in CGI machining, is thus reduced. The MAM configuration employing feed-direction modulation appears feasible for implementation at high speeds and offers a potential solution to this challenging class of industrial machining applications.

Keywords Machining · Tool wear · Modulation · Compacted graphite iron (CGI) · Cubic boron nitride (CBN)

1 Introduction

Compacted graphite iron (CGI), belonging to the family of cast irons, has emerged as a candidate material to substitute gray cast iron (CI) in engine block applications for diesel engines because of superior mechanical properties, and improved strength-to-weight and stiffness-to-weight characteristics. The tensile strength and fatigue strength of CGI are nearly double those of CI, the elastic modulus is about 35 % higher than that of CI, and the thermal conductivity is about 25 % smaller than that of CI [1, 2]. These properties enable CGI-based engines to operate at higher cylinder pressures and temperatures, with better fuel economy and lower emissions. While castability of CGI is similar to that of CI, its poor machinability in continuous cutting at high speeds is a challenge for wide ranging implementation in diesel engines. The machinability problem is addressed in the present study.

The major difference between CGI and CI, accounting for the improved mechanical properties, is in graphite shape and 3D morphology [2]. The graphite in CI typically appears as randomly oriented flakes, thin and long, and with smooth surfaces and sharp edges. The sharp edges are sources of stress concentration facilitating crack initiation, while the smooth surfaces facilitate crack propagation. In contrast, the graphite in CGI is present as vermicular particles which are thicker and shorter than the flakes in CI. More importantly, the vermicular particles have round edges which reduce stress concentration. When characterized in 3D, the graphite particles in CGI are actually connected with a coral-like morphology. Consequently, there is stronger bonding between the graphite and iron matrix. This coupled with inhibition of fracture due the graphite morphology results in increased strength and ductility/toughness.

In spite of attractive structural properties for diesel engines, CGI has not found widespread use to date in the automotive industry. The major barrier is its poor machinability, as quantified by tool wear/life, under conditions typical of automotive production. When performing continuous cutting operations, e.g., turning, boring, and

Y. Guo · J. B. Mann · H. Yeung · S. Chandrasekar (✉)
Center for Materials Processing and Tribology,
School of Industrial Engineering, Purdue University,
West Lafayette, IN 47906, USA
e-mail: chandy@purdue.edu

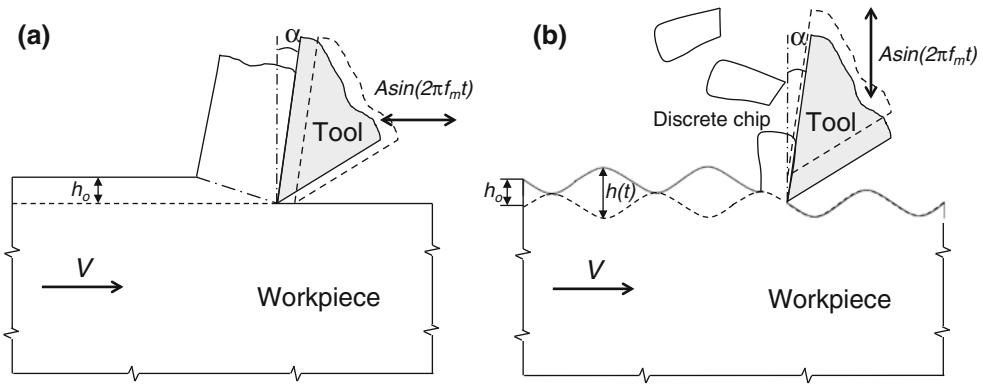

Fig. 1 Schematic of modulation-assisted machining (MAM) **a** velocity-modulation **b** feed-modulation. α is the tool rake angle, and h_o is the undeformed chip thickness (feed in turning)

using polycrystalline cubic boron nitride (CBN) tools at high speeds (500 m/min or more) typical of current transfer lines, the tool life is often 20 times lower when cutting CGI as against CI. Even in continuous cutting of CGI at low speeds (150–250 m/min) or milling (interrupted cutting) at high speeds, the tool life is $\sim$50 % smaller than for CI [3]. Solutions proposed to overcome the machinability barrier such as cutting at lower speeds and re-designing the machining process to use rotary tools, although partially effective, have not solved the problem of cost-effective machining of CGI [4].

The present study describes a somewhat unconventional approach to address the challenge of CGI machining at high speeds. The approach utilizes modulation-assisted machining (MAM) that incorporates controlled superimposition of a low-frequency modulation (frequency $<$ 1,000 Hz and amplitude $<$ 200 μm) to the conventional machining (CM) process (Fig. 1). The initial results showed that CBN's tool life in MAM of CGI can be at least an order of magnitude greater than that in the CM (i.e., without modulation). The improvements are a direct consequence of mitigation of the factors controlling thermochemical wear at the tool–chip–work contacts.

2 Background: CBN Tool Wear in Machining of CGI

The underlying causes and mechanisms contributing to high CBN tool wear when machining CGI has received a great attention [2, 3, 5–7]. While there is still debate about the micromechanisms of wear that are operative, the development of cost-effective machining methods for CGI does not have to await a resolution of this debate. For the present study, it will suffice to consider the wear modes only at a macroscopic level, identifying the principal factors leading to the enhanced tool wear. The tool–chip contact in CM is characterized by intimate contact (real area $\approx$ apparent area) between nascent surfaces sliding against each other, often at high speeds (>500 m/min) as in the case of machining of cast irons. Large shear and normal stresses, and elevated temperatures (>800 °C with CGI), are typical of this contact. Together, these contact conditions are conducive to activation of thermochemical wear mechanisms including diffusion, chemical reaction, and oxidation [8]. The dominant wear mode in the CBN–CGI system has been shown to be thermochemical in nature, accentuated by the lack of formation of a manganese sulfide (MnS) barrier layer at the tool–chip interface [5, 6]. Such a layer is seen to prevail when machining CI at high speeds resulting in low tool wear. The role of the MnS layer in reducing wear appears to be twofold. First, it acts as a barrier layer protecting the tool edges and faces by suppressing thermochemical wear along the tool–chip interfaces. Second, the layer has "self-lubricating" characteristics providing for some lubrication of these interfaces which are otherwise difficult to access for fluids because of the severity of the contact. Of course, MnS is also well known for promoting free machining characteristics. The lack of a MnS layer in CGI cutting is due to the much lower concentration of sulfur and MnS in CGI than in CI. This is because the development of the vermicular graphite morphology requires minimization of free sulfur which is accomplished by adding magnesium to the cast iron melt. Magnesium bonds strongly with the sulfur to form magnesium sulfide (MgS) inclusions, thus minimizing the free sulfur, while simultaneously precluding formation of MnS inclusions typical of conventional cast irons.

The nature of the chip formation that occurs with CGI is another contributing factor to the enhanced wear [7]. Because of the relatively brittle nature of CI, the chips produced are quite discontinuous and discrete resulting in a less severe contact condition prevailing along the chip–tool interface. In contrast, chips from CGI tend to be less discontinuous and longer because of the greater ductility of the CGI. This results in a more severe contact condition and higher temperatures along the tool–chip interface, conditions conducive to thermochemical wear. Thus, the very factors that contribute to CGI's unique structural properties are a barrier to its cost-effective machining.

Much effort has been devoted to addressing the problem of excessive tool wear in CGI machining. Enhancing

machinability by modification of the composition to increase sulfur content has been suggested but this would negate the basic concept behind the improved structural properties of CGI. Attempts to create the stable MnS barrier layer along the tool–chip contact in high-speed machining using external introduction of a sulfur-based lubricant have been unsuccessful, as have been approaches based on use of tool materials other than CBN. A third approach to make the cutting somewhat interrupted, utilizing tooling concepts, such as a rotary insert or a boring tool with multiple inserts, has met with limited success. The rotary tool uses a circular insert that is free to rotate on its axis resulting in the cutting region of the insert continuously changing with time; this reduces the intensity of exposure of the cutting regions to mechanical and thermal loads. However, this concept has two drawbacks, one arising from the relatively large size of the rotary tool which precludes its application in machining of small diameter cylinder bores, and the second related to rapid wear of the bearings used to enable the rotary action [4].

A solution to CGI machining is suggested if attention is focused on the factors that alleviate thermochemical wear in general rather than on the micromechanisms peculiar to CGI machining. Thermochemical wear should be reduced by lowering the contact temperature and time at this temperature, reducing the severity/intimacy of tool–chip contact, and promoting conditions conducive for fluid action along the contact. As MAM under conditions of discrete chip formation (see Sect. 3) can accomplish all of these even at high speeds, a significant opportunity has emerged for cost-effective machining of CGI.

3 Modulation-Assisted Machining

The application of a controlled superimposed modulation to machining resulting in MAM is of two types, with fundamentally different kinematics: a) modulation in the direction of cutting velocity—velocity-modulation (Fig. 1a) and b) modulation in the direction of tool–feed or undeformed chip thickness—feed-modulation (Fig. 1b). Both types of modulation change the nature of tool–work engagement and/or chip formation, but not the material removal rate (MRR) which is determined only by the conventional (baseline) machining conditions.

3.1 Velocity-Modulation

Figure 1a, shows a schematic of machining with sinusoidal velocity-modulation. The undeformed chip thickness (h_o) is constant, but the cutting velocity (V) varies continuously in each cycle of modulation. The tool–chip contact is disrupted every modulation cycle when $2\pi f_m A > V$, where f_m is the modulation frequency, and $2A$ is the peak-to-peak amplitude. This disruption of the tool–chip contact, together with penetration of fluid into the contact and a 2–3 fold reduction in the friction therein at these conditions, has been confirmed in the low-frequency regime ($f_m < 1$ kHz) in various cutting configurations [9, 10]. The experiments also showed that in the absence of the modulation, the tool and chip were in intimate contact with little visible penetration of the fluid (applied) into the contact region [9, 11]. An interesting demonstration of velocity-modulation machining, albeit in the ultrasonic modulation (high frequency) regime, is diamond turning of steel at relatively low workpiece speeds (0.02–0.07 m/s) with small tool wear [12]. In CM, this process is characterized by excessive wear because of the chemical affinity between iron and diamond. Disruption of the severity of the tool–chip contact and lower interfacial temperatures with the superimposed vibration is likely the reason for this wear reduction [13].

While velocity-modulation is effective at disrupting the severity of the tool–chip contact, this approach has major limitations in implementation. First, the disruption condition $2\pi f_m A > V$ is difficult, if not impossible, to realize in practice even at ultrasonic frequencies, except at the very low end of machining speeds ($V < 0.5$ m/s), due to dynamic system level constraints [12, 14]. Second, this approach does not result in discrete chips since h_o is essentially constant throughout the cutting (Fig. 1a). Finally, this modulation is kinematically difficult to impose in processes such as drilling and boring as it would require a superimposed oscillation in the rotation direction. Of more general applicability is the feed-modulation of low frequency, wherein discrete chip formation and disruption of the tool–chip contact can be realized concurrently even at high machining speeds ($V \gg 0.5$ m/s).

3.2 Feed-Modulation

Figure 1b, shows a schematic of machining with sinusoidal modulation, $Asin(2\pi f_m t)$, superimposed parallel to h_o (i.e., tool feed in turning or boring). This is the MAM configuration that is of interest to the present study. Unlike CM ($f_m = 0$), the undeformed chip thickness ($h(t)$) varies with time (t). When A is sufficiently large, then $h(t)$ becomes equal to zero for some time in each modulation cycle, resulting in "discrete chips" at the rate of f_m per second. The tool–chip–work contacts are concurrently disrupted at the same rate [15]. The critical value of A for discrete chip formation can be estimated based on when $h(t)$ becomes zero in a modulation cycle. For continuous machining with a single cutting-edge tool as in lathe turning, this condition is given by [16]

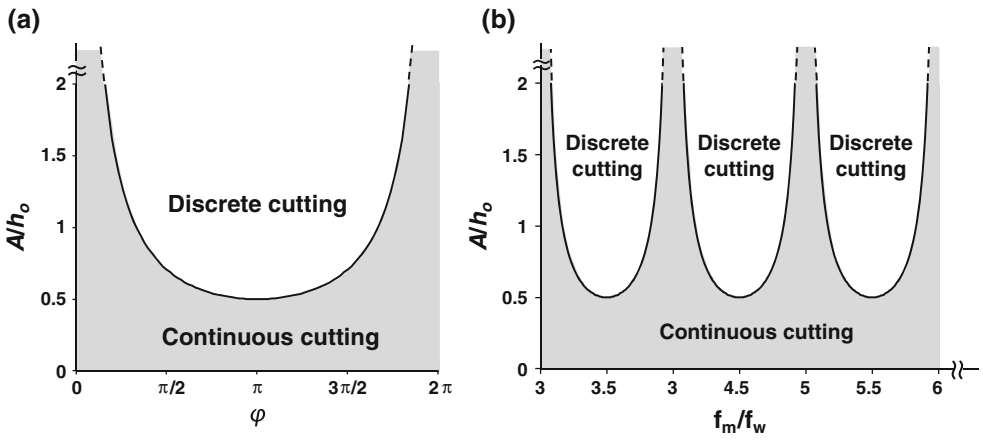

Fig. 2 Cutting regimes of MAM in **a** $\varphi - A/h_o$ space and **b** $f_m/f_w - A/h_o$ space. The discrete cutting regime is concurrent with disengagement of the tool from the workpiece in each modulation cycle

$$A/h_o = 1/[2\sin(\varphi/2)] \tag{1}$$

with

$$\varphi = 2\pi\,(f_m/f_w - INT[f_m/f_w]), \quad 0 \le \varphi < 2\pi \tag{2}$$

where f_w is workpiece rotational frequency, and "*INT[ ]*" denotes the integer part of the value.

Fig. 2a shows the dependence of A/h_o on φ. Since φ depends only on f_m/f_w (Eq. 2), A/h_o can also be plotted as a function of f_m/f_w (Fig. 2b); in this framework, the single curve of Fig. 2a decomposes into multiple U-curves, three of which are shown. These curves mark the boundary between continuous (i.e., $h(t) > 0$) and discrete cutting. For MAM conditions outside the U-curve (shaded area), the tool is always engaged with the workpiece, and the cutting is continuous despite the modulation. MAM conditions inside the curve (unshaded area) result in discrete chips and disruption of the tool–chip contact in each cycle of modulation. Points along the curves represent the minimum amplitude required to effect discrete chip formation at the respective f_m/f_w. The global minimum or the smallest value of A for discrete chip formation is $2A = h_o$, and occurs when $\varphi = \pi$, i.e., $f_m/f_w = \frac{1}{2}(2N + 1)$, with N being an integer (Fig. 2 and Eq. 1). This condition, $f_m/f_w = \frac{1}{2}(2N + 1)$ and $2A = h_o$, is labeled as the optimum modulation condition, since this condition results in the smallest amplitude for disruption of the tool–chip contact. The length of time during which the tool is disengaged from the workpiece can be controlled by setting A greater than the critical amplitude for disruption; the larger the value of A the greater is the time for which the tool remains disengaged from the workpiece. Fig. 2 also shows instances where discrete chip formation can never be realized even with modulation of arbitrarily large A. At the asymptotic ends of the U-curves corresponding to $f_m/f_w = N$, successive cutting cycles are "in phase," and discrete chip formation is never realized regardless of A. Instead, a continuous chip should be expected at all machining conditions.

Modulation conditions for discrete chip formation with multiple cutting edge tools (e.g., drilling) can be established analogously [16]. These observations pertaining to discrete chip formation and disruption of tool–chip contact have been verified in experiments with ductile alloys, including direct observations of the chips formed, and their shapes and dimensions at various frequency–amplitude conditions [16].

The amplitude conditions for discrete chip formation and contact disruption can be implemented even at high speeds in MAM with feed-modulation. For example, since amplitudes as large as 0.2 mm can be achieved using piezo-type actuators for f_m <1,000 Hz, this amplitude condition can be effected even at speeds of ~15 m/sec and feed rates of up to 0.4 mm per revolution (per Eq. 1), making it especially well suited for industrial practice. Hence, this type of MAM was selected for the study of CBN tool wear in CGI machining.

4 Experimental

A series of experiments was carried out for single-point turning of CGI cylinder liners (SinterCast) at high speeds to determine the type of effect that MAM has on tool wear in the CBN–CGI system. The tests were done with and without the application of modulation in the presence of air–mist lubrication (Mobilmet Omega Cutting Oil). The machining conditions were feed $h_o = 0.05$ mm/rev, depth of cut (doc) = 1 mm, and cutting speed $V = 550$ m/min at 1,500 rpm ($f_w = 25$ Hz), resulting in an MRR of ~27500 mm^3/min. These baseline conditions were kept the same in both the CM and MAM tests, and are similar to those of interest to cast iron machining in the industrial sector. The modulation was provided by a large-scale, prototype modulation device (M4 Sciences LLC) employing piezoelectric actuation. It was configured to hold a 19.05 mm-diameter boring bar that was

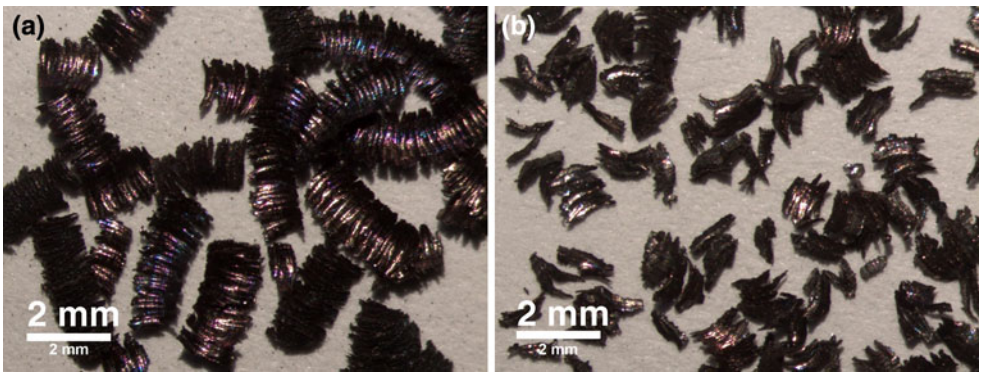

Fig. 3 Chips produced in **a** conventional machining (CM) and **b** MAM. The average chip lengths in CM and MAM are 3.1 mm and 0.6 mm, respectively. The chip colors suggest a higher temperature in CM. CBN–HTM; $V = 550$ m/min; $h_o = 0.05$ mm/rev; doc = 1 mm; $f_m/f_w = 4.5$

used to machine the outside diameter of the cylinder liners. Pictorial details of the MAM kinematical configuration may be found elsewhere [10, 16]. The modulation conditions were $f_m = 112.5$ Hz and $A \sim 0.03$ mm, this selection being guided by the piezo-actuation characteristics of the modulation device. For these modulation conditions, the f_m/f_w ratio is 4.5, and A is sufficiently large ($2A > h_o$) enabling discrete chip formation (Eq. 1) as characterized by relatively "short" chips (Fig. 3). The chips produced in MAM had an average length of $\sim$0.6 mm (Fig. 3b), while those from CM had a length of $\sim$3.1 mm (Fig. 3a).

The Brinell hardness of the CGI used was 217 HB. The CBN inserts (Diamond Innovations) in brazed form were of two types: (1) HTM with 50 % volume CBN, and (2) BZN 9100 with 90 % volume CBN. The latter is considered as "harder" grade because of its higher CBN content. The wear of the tool was characterized by measurements of flank wear land height along the main flank and nose region, and of crater wear using an optical microscope. Flank wear-based life criteria are the most commonly used in CI machining. These measurements were made at intervals of $\sim$2.6 min of cutting, corresponding to a cut volume of $\sim$71,500 mm^3 between two consecutive measurements. Before each measurement, the insert was cleaned ultrasonically in isopropyl alcohol. Photographs were taken of the different wear regions. The wear was assessed by studying the evolution of flank wear ($VB_{\max}$) with cutting time, where $VB_{\max}$ is the usual maximum flank wear land height. This characterization was done along both the tool nose and the main flank face. A limited series of wear tests was also carried out with lubricants/fluids such as MoS_2, cutting oil (Mobilmet Omega Cutting Oil), and water. The MoS_2 was applied in slurry form before and during the cutting, and the oil/water as air–mist during the cutting. The chips produced in the experiments were characterized in terms of morphology and microstructure.

5 Results

Figure 4 shows the evolution of $VB_{\max}$ with time for HTM–CBN in CM and MAM. Results from three different tests are plotted for each of the two machining cases, demonstrating the extraordinary reduction in tool wear with MAM. The error bars (standard deviation) for the wear data in MAM are much smaller than those in CM indicating that the progression of wear in MAM is quite stable and repeatable. This wear evolution can be presented in terms of volume of material cut by using the MRR value of 27,500 mm^3/min. The following observations can be made from Fig. 4, and the optical microscope pictures of Fig. 5 which show typical wear patterns along the main flank, nose and crater regions of the tools.

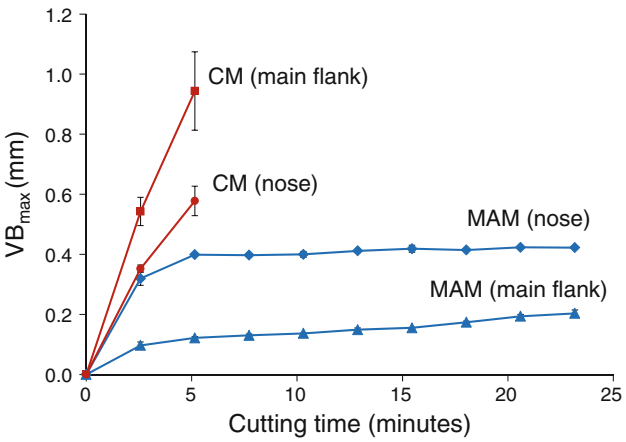

Fig. 4 Variation of maximum flank wear land width ($VB_{\max}$) with cutting time. In CM, the maximum wear occurs on the main flank, while in MAM, it occurs on the tool nose (see Fig. 5). For comparison, the wear on the main flank in MAM is also shown. The tool life is <3 min in CM while in MAM, it is >20 min. CBN–HTM; $V = 550$ m/min; $h_o = 0.05$ mm/rev; doc = 1 mm; $f_m/f_w = 4.5$; MRR = 27500 mm^3/min. Note that the *error bars* for the MAM data are too small to be seen in the plot

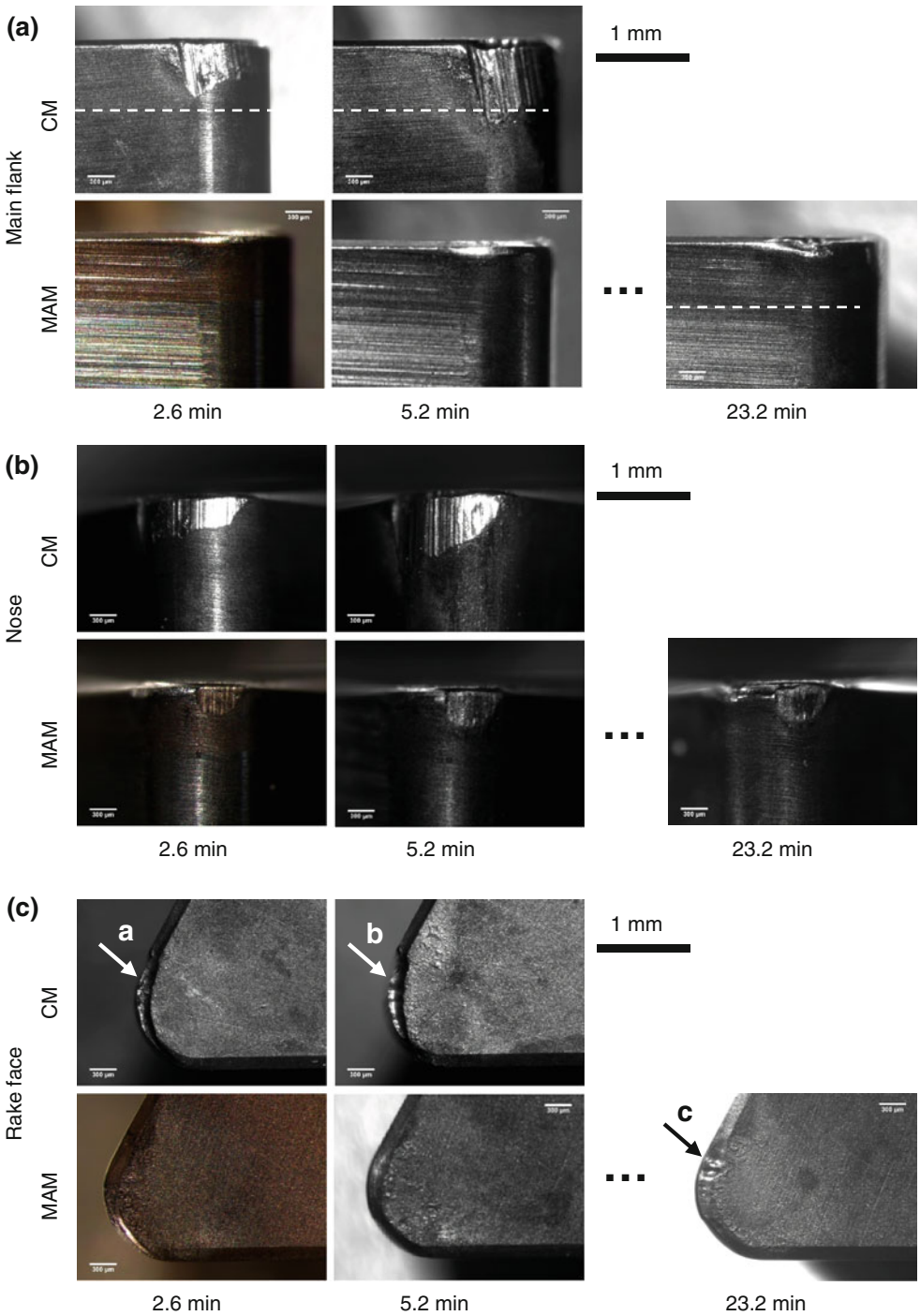

Fig. 5 Optical microscope images of tools showing wear on **a** main flank **b** tool nose, and **c** rake face in CM and MAM. CBN–HTM; $V = 550$ m/min; $h_o = 0.05$ mm/rev; doc = 1 mm; $f_m/f_w = 4.5$; MRR = 27,500 mm^3/min

The flank wear is initially rapid in both the CM and MAM tests; this likely is a period of "running in" wherein tool–workpiece conformity is established. Subsequently, the wear in MAM progresses only at a very small steady rate ($\sim$5 μm/min), whereas in CM it continues to be rapid without showing the steady (low rate) wear stage. In fact, within about 4 min of testing, the wear land in CM breached the CBN (brazed) layer, penetrating into the underlying carbide substrate at a depth of $\sim$0.8 mm from the original rake face of the tool (dotted line in Fig. 5a) and destroying the integrity of the cutting edge. In contrast, the flank wear in the MAM tests remains well within the CBN layer (Fig. 5a) and in the small wear rate condition even after $\sim$23 min of cutting (Fig. 4), at which stage these tests were stopped. The tool life for MAM (>23 min) is at least 10 times that for CM ($\sim$2.5 min). The location of the maximum wear land in MAM is at the tool nose (Fig. 5b) while in CM it is along the main flank adjoining the tool

nose (Fig. 5a). This difference in the wear land location between CM and MAM likely arises from differences in the aforementioned tool–workpiece conformity during running-in. The variation of VB_{max} with time in MAM is similar for both the nose and flank regions, i.e., an initial somewhat rapid wear followed by the steady small wear, but the VB_{max} values in themselves are much smaller along the main flank (Fig. 4).

The evolution of crater wears in CM and MAM is shown in Fig. 5c. In less than 5 min of cutting in CM, the crater on the rake face has progressed to and encompassed the main cutting edge (see the arrows a and b in Fig. 5c), severely damaging its cutting integrity. In contrast, there is little by way of visible crater wear at an equivalent stage of cutting in MAM. While a crater does develop with further cutting, it is confined to a small region (arrow c), and its depth is not of significant dimensions even after 23 min of cutting.

Similar large reductions in flank wear with MAM relative to CM were observed in tests carried out with the second type of CBN–BZN 9100. Figure 6 shows the flank wear data for CM and MAM for this CBN type. The data are very much analogous to those observed with the HTM–CBN (Fig. 4), with one important difference: the VB_{max} values and the steady wear rate ($\sim$2.2 μm/min) are even smaller for the BZN 9100 in MAM. The tool life of BZN 9100 in MAM (>46 min) is more than 20 times that in CM ($\sim$2 min). The lower wear of BZN 9100 relative to HTM–CBN is undoubtedly due to this insert being much harder, a consequence of its much higher CBN content ($\sim$90 %).

An assessment of the effect of fluid type on wear was carried out using a short-duration (2.6 min) MAM test. Figure 7 summarizes the results in the form of a bar chart for VB_{max}. Data for CM with cutting oil are also shown for comparison. It is clear that the wear reduction by MAM

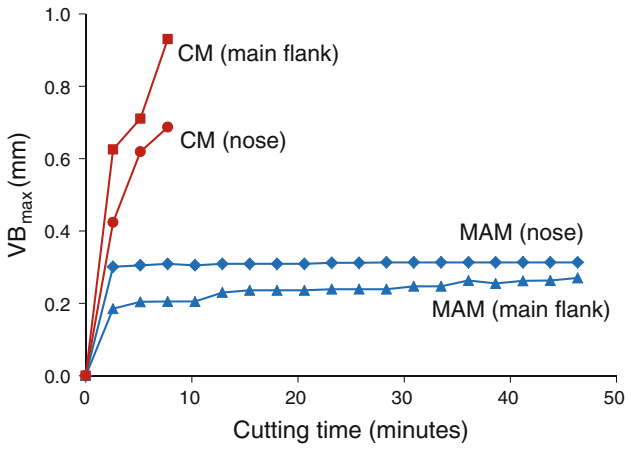

Fig. 6 Variation of VB_{max} with cutting time. CBN–BZN9100; $V = 550$ m/min; $h_o = 0.05$ mm/rev; doc = 1 mm; $f_m/f_w = 4.5$; MRR = 27,500 mm^3/min

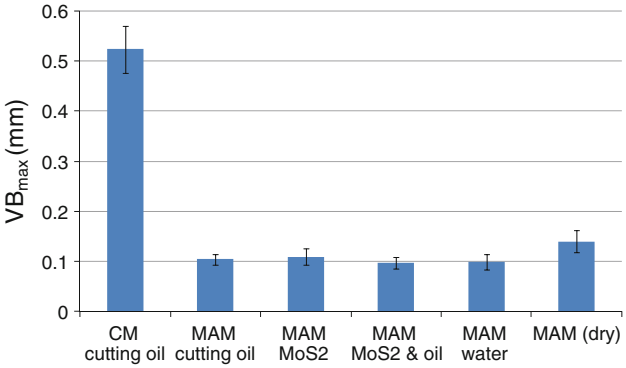

Fig. 7 VB_{max} with different fluids/additives. The wear was measured on the main flank after 2.6 min of cutting. CBN–HTM; $V = 550$ m/min; $h_o = 0.05$ mm/rev; doc = 1 mm; $f_m/f_w = 4.5$

transcends fluid types, with all of the fluids tested showing similar large flank wear reductions compared with CM. Indeed, a large wear reduction is observed even when cutting dry in air; the level of this reduction is somewhat less than with the fluids. While these wear data are necessarily from the earlier stages of cutting, the general, across-the-board, steep reduction in wear observed in MAM is quite heartening and consistent with the more extensive, steady-state wear data presented earlier.

6 Discussion

The experimental results have shown that the wear of CBN tools when cutting CGI at high speeds is significantly lower in MAM compared with conventional machining (CM) (Figs. 4, 6). Based on the results, the typical tool life in MAM is seen to be at least an order of magnitude greater than the corresponding life in CM and represents an extraordinary improvement in wear performance for cutting tools. This is also a conservative estimate of the enhancement in life since extrapolation of the MAM data in the steady wear regime in Figs. 4 and 6 to $VB_{max} = 0.6$ mm (typical life criterion [17]) suggests tool life values in excess of 60 min. The reduction in tool wear in the presence of modulation is undoubtedly a consequence of the discrete chip formation cutting conditions disrupting the tool–chip contact, and occurs with just air–mist lubrication. A plausible hypothesis as to the mechanism of wear reduction is that the disruption reduces the severity of the tool–chip contact, including enabling a very thin layer of fluid to be active in the contact zone, and lowers the temperature in the machining zone. Under such conditions, the wear rate is determined primarily by the relative hardness of the two bodies in contact, as in many sliding contact situations [18]; since CBN is much harder than CGI, the wear rate of CBN should then be small. This

hypothesis is supported by the experimental observations and related inferences.

The modulation frequency (f_m) in the MAM experiments was set such that f_m/f_w was 4.5; consequently, the tool–chip contact was disrupted 4.5 times per revolution of the workpiece. Visual and optical observations (Fig. 3) indicated that the chips formed in MAM were much smaller than in CM, and the reduction in chip lengths was consistent with the frequency of disruption of the tool–chip contact. High-speed photography with a model cutting system has shown that MAM, let it be of the velocity-modulation or feed-modulation type, facilitates fluid access to the cutting zone [9]. In contrast, there is negligible penetration of fluid into the tool–chip contact region in CM as inferred from measurements of fluid film's thickness made using luminescent molecule sensors [11]. Thus, the tool–chip contact in MAM is likely to be much less intimate than in CM, and similar to conventional sliding contacts where the real area of contact is a very small fraction of the apparent (geometric) area of contact.

The cutting zone temperatures in MAM appear to be lower than in CM, and this should further alleviate thermochemical wear. Evidence for this lowering of the temperature may be seen in the colors of the chips resulting from MAM and CM (Fig. 3). The CM chips (Fig. 3a) show a multiplicity of colors (e.g., blue, purple, violet, etc.) typically resulting from scattering from thin oxide films present on the chip surfaces; this is usually indicative of cutting temperatures exceeding the oxidation threshold in the process of chip formation. Such colors are much less prevalent in the MAM chips (Fig. 3b). Calculations of machining zone temperature suggest a reduction in temperature of at least 20 % for the case of MAM [19], this reduction resulting purely from the periodic disruption of the tool–work contact and associated modification of the time history of the heat flux. The periodic disengagement of the tool from the workpiece limits the time for which the tool–chip contact is exposed to an elevated temperature, minimizing another driving force for thermally activated wear mechanisms. For the MAM conditions ($f_m \sim 100$ Hz and $A \sim 0.03$ mm) used in the present study, this time at temperature is less than 10 ms. Recent measurements of forces and specific energy in our laboratory using a force sensor (natural frequency in the mounted condition $\sim$5 kHz), albeit, in MAM of ductile Cu and Al alloys, have shown that energy dissipation in MAM can be at least 25 %, and often 40 %, less than in CM, due to a reduction in the strain associated with chip formation [15] and in the friction at the tool–chip contact [9]. Similar reduction in forces/energy has also been reported in the ultrasonic vibration-assisted regime [13]. This energy reduction should result in a significant lowering of the heat flux. If this is incorporated into the aforementioned calculations, then an even larger reduction in temperature is envisaged for MAM. Additional anecdotal evidence for lower temperatures in MAM comes from some visual observations made during the CGI machining. A dense cloud of smoke, likely resulting from degradation of the cutting fluid at elevated temperatures, was observed in the vicinity of the machine tool in the conventional machining but not in the MAM, translating the temperature changes into quite a dramatic visual effect. The reductions in temperature should also enhance the fluid action (lubrication and cooling) in cutting by limiting degradation of fluid properties. These observations should be further validated by measurement of cutting temperatures planned in the near future.

The present experiments involved MAM with f_m/f_w set at 4.5. Increasing or decreasing this ratio will cause the tool to disengage from the workpiece more or less frequently. Amplitude and actuator characteristics will set an upper limit to this ratio in practice, but further study is needed to determine the optimum setting of this ratio based on considerations of tool life and cutting temperature. While these issues will be explored in the near future, the extraordinary reduction in wear and enhancement of tool life observed suggest that MAM with feed-modulation is a solution to the problem of cost-effective machining of CGI at high speeds typical of industry applications.

7 Conclusions

Modulation-assisted machining (MAM) resulting in discrete chip formation and periodic disruption of the tool–chip–work contact is shown to reduce significantly, the wear of CBN tools in machining of compacted graphite iron (CGI). The resulting tool life is at least one order of magnitude greater than that measured in conventional machining at equivalent material removal rates. This extraordinary reduction in wear appears to be a consequence of a reduction in the severity of the tool–chip contact conditions in MAM: reduction in intimacy of the contact, lower cutting temperatures, and reduced-time exposure to elevated temperatures, enhanced fluid action, and formation of discrete chips. Such conditions reduce the propensity for thermochemical wear of CBN, the principal wear mode operative in CGI machining at high speeds. The MAM configuration employing feed-direction modulation appears feasible for implementation in CGI machining at high speeds, thereby offering an economically viable machining solution to this challenging class of industrial machining applications.

Acknowledgments This study was supported in part by Diamond Innovations, Inc. (Columbus, Ohio, USA) and a Bilsland fellowship

to Yang Guo. We thank M4 Sciences LLC for providing the prototype large-scale MAM system used in the study.

References

1. Dawson, S.: Compacted graphite iron: mechanical and physical properties for engine design. Paper presented at Materials in Powertrain VDI, Dresden, Germany. SinterCast Tech. Publication (1999)
2. Dawson, S., Hollinger, I., Robbins, M., Daeth, J., Reuter, U., Schulz, H.: The effect of metallurgical variables on the machinability of compacted graphite iron. SAE Tech. Pap. Ser. 2001-01-0409 (2009)
3. Abele, E., Sahm, A., Schultz, H.: Wear mechanism when machining compacted graphite iron. Ann. CIRP **51**, 53–56 (2002)
4. Zelinski, P.: Surpassing the speed limit in CGI. Mod. Mach. Shop **76**, 102–103 (2003)
5. Gastel, M., Konetschny, C., Reuter, U., Fasel, C., Schulz, H., Riedel, R., Ortner, H.M.: Investigation of the wear mechanism of cubic boron nitride tools used for the machining of compacted graphite iron and grey cast iron. Int. J. Refract. Met. Hard Mater. **18**, 287–296 (2000)
6. Heck, M., Ortner, H.M., Flege, S., Reuter, U., Ensinger, W.: Analytical investigations concerning the wear behavior of cutting tools used for the machining of compacted graphite iron and grey cast iron. Int. J. Refract. Met. Hard Mater. **26**, 192–206 (2008)
7. Tasdelen, B., Escursell, M., Grenmyr, G., Nyborg, L.: Machining of gray cast irons and compacted graphite iron. In: Swedish Production Symposium. pp. 1–6 (2007)
8. Shaw, M.C.: Metal cutting principles. Clarendon Press, Oxford (1984)
9. Moscoso, W., Olgun, E., Compton, W.D., Chandrasekar, S.: Effect of low-frequency modulation on lubrication of chip-tool interface in machining. J. Tribol. **127**, 238–244 (2005)
10. Mann, J.B., Saldana, C., Moscoso, W., Compton, W.D., Chandrasekar, S.: Effects of controlled modulation on interface tribology and deformation in machining. Tribol. Lett. **35**, 221–227 (2009)
11. Huang, C., Lee, S., Sullivan, J.P., Chandrasekar, S.: In situ measurement of fluid film thickness in machining. Tribol. Lett. **28**, 39–44 (2007)
12. Moriwaki, T., Shamoto, E.: Ultraprecision diamond turning of stainless steel by applying ultrasonic vibration. Ann. CIRP **40**, 559–562 (1991)
13. Brehl, D.E., Dow, T.A.: Review of vibration-assisted machining. Precis. Eng. **32**, 153–172 (2008)
14. Kumabe, J.: Vibration cutting—basic principle and application. Jikkyo Shuppan Books, Japan (1979)
15. Mann, J.B., Saldana, C., Chandrasekar, S., Compton, W.D., Trumble, K.P.: Metal particulate production by modulation-assisted machining. Scr. Mater. **57**, 909–912 (2007)
16. Mann, J.B., Guo, Y., Saldana, C., Compton, W.D., Chandrasekar, S.: Enhancing material removal processes using modulation-assisted machining. Tribol. Int. **44**, 1225–1235 (2011)
17. Boothroyd, G.: Fundamentals of metal machining and machine tools. McGraw-Hill, New York (1975)
18. Hutchings, I.M.: Tribology: friction and wear of engineering materials. Arnold, London (1992)
19. Kountanya, R.: Cutting tool temperatures in interrupted cutting—the effect of feed direction modulation. J. Manuf. Process **10**, 47–55 (2008)